Transient Turbulent Flow Simulation with Water Model Validation and Application to Slide Gate Dithering

Rui Liu and Brian G. Thomas
Department of Mechanical Science and Engineering,
University of Illinois at Urbana-Champaign
1206 W. Green Street,
Urbana, IL 61801 USA
Phone – (217) 333-6919
Fax – (217) 244-6534
Email: bgthomas@illinois.edu

Bruce Forman and Hongbin Yin
ArcelorMittal Global R&D East Chicago Center,
3001 East Columbus Drive,
East Chicago, IN 46312 USA
Phone – (219) 399-5213
Fax – (219) 399-3899
Email: bruce.forman@arcelormittal.com, Hongbin.Yin@arcelormittal.com

ABSTRACT

Slide gate dithering can reduce nozzle clogging and sticking during continuous casting, but also influences transient flow in the mold and meniscus level fluctuations. In this work, a semi-analytical model was first developed and validated to predict nozzle flow rate from slide-gate opening position. A transient CFD model of 3-D turbulent flow was then validated with surface velocity measurements in a water model. Finally, transient two phase flow simulations were performed to investigate nozzle and mold flow pattern variations during gate dithering, with Upper Tundish Nozzle (UTN) hot argon injection rate and bubble size calculated with a porous-flow nozzle-refractory model, and steel flow rate calculated using the gate-position-based model. The transient simulation shows liquid steel jet wobbling and periodic gas-rich pockets entering the mold region during dithering. The mold level oscillates periodically during dithering, with about the same frequency, and the amplitude of the mold level fluctuations increases in proportion to the gate dithering stroke. Validation is provided by the match between the predictions and plant measurements of unfiltered mold level history.

Key words: slide-gate dithering, gate-position-based model, porous-flow model, Eulerian-Eulerian model

INTRODUCTION

Nozzle clogging occurs during continuous casting of steel, which limits production, can send large inclusions into the mold when clogs dislodge, and is detrimental to the flow pattern in the mold region. Clogging can increase detrimental meniscus level fluctuations [1], and causes defects in the final product, including surface defects, slag entrainment via many different mechanisms [2], and internal inclusions. Sudden release of a sticking slide gate after short periods of inactivity is another cause of detrimental flow variations. Continuous "dithering" of the slide-gate, by oscillating the gate-opening area at a small amplitude and high frequency, has been proposed to avoid these problems. However, slide-gate dithering itself produces periodic alteration of the liquid steel flow, which has received little previous study.

Transient flow in continuous casting has been investigated in a few modeling studies, using 3-D Unsteady Reynolds Average Navier-Stokes (URANS) models [3-5] and recently Large-Eddy-Simulation models [6-7]. For example, Huang and Thomas [5] developed a 3-D finite-difference model to simulate transient argon-steel two phase flow patterns in the mold, and found large scale vortex shedding phenomenon during the transition from asymmetric flow of nozzle clogging to steady symmetrical flow. Unfortunately, the time-variation of liquid steel flow rate is not easy to measure, but is crucial to investigate phenomena during realistic transient flow

events. A modeling approach to determine the flow rate based on stopper-rod position was recently developed by Liu et.al. [4] and applied to study the effects of stopper rod movements on flow that eventually lead to sliver formation at ArcelorMittal Dofasco even while the casting speed was kept constant.

Since argon gas is usually injected into conventional casters to prevent clogging and reoxidation of the liquid steel with entrained ambient air [1], argon-steel two phase flow must be modeled. In addition to the added modeling complexity, this task has the practical difficulty of obtaining the hot gas flow rate entering the nozzle and the resultant bubble size distributions after injection. Most previous work with argon-steel two phase flows converts the measured gas flow rate at standard condition (room temperature and pressure) into the hot argon flow rate, using the ideal gas law to account for gas expansion to the casting temperature [5]. However, during real casting processes, gas leakage might occur and the hot argon flow rate entering the nozzle is not easy to find. Furthermore, as investigated by Shi and Thomas [8], bubble size also plays an important role in determining the flow pattern argon-steel two phase simulations, which is also related to the gas flow distribution at UTN inner surface. Thus, a model for gas flow through nozzle refractory is needed to provide proper argon gas inlet boundary condition for argon-steel two phase flow simulation in a caster.

This work presents a system of models to investigate transient flow during multiphase continuous casting, and applies it study slide-gate dithering. First, the flow-rate change during the process is calculated via a gate-position-based model, which is validated with water model experiments. Next, the argon volumetric flow rate in hot condition is determined by a porous-flow model of the gas flowing through heated refractory. Then, a transient, three-dimensional, CFD model is validated against velocity measurements in water model experiments. Finally the 3-D transient Eulerian-Eulerian multiphase model is applied to gain new insight into argon-steel two phase flow in the SEN and mold region during the dithering process, based on inlet conditions from the previous models.

MODEL DESCRIPTION AND VALIDATION

A system of models are developed, validated and utilized to investigate the dithering process, including an analytical model to predict SEN liquid steel flow rate based on slide-gate position, a porous-flow model to calculate the argon flow rate in hot condition based on the measured back pressure, and an Eulerian-Eulerian model to simulate the argon-steel two-phase flow in the SEN and mold region. The computational domains assume left-right symmetry, modeling half of the SEN and mold regions.

Gate-Position-Based Model for SEN Liquid Steel Flow Rate Calculation

The slide-gate opening position controls the liquid steel flow rate through the SEN. This flow rate is determined by the pressure head losses over the system. A semi-analytical model has been developed to predict flow rate as a function of nozzle geometry, slide-gate position, tundish height, and argon gas injection rate. The model is based on Bernoulli's equation and empirical relations, similar to a previous stopper-position-based model [4]. The model is validated using water model experiments performed at ArcelorMittal Global R&D at East Chicago. Liquid steel flow rate through the SEN, Q_{SEN} (m^3/s), is calculated as follows:

$$Q_{SEN} = A_{eff}\sqrt{\frac{2\left(H_1+H_2\right)g}{\left(\frac{A_{SEN}}{A_{port}}-1\right)^2+f\frac{L_{SEN}}{D_{SEN}}+\left(\frac{1}{\mu}-1\right)^2\left(\frac{A_{SEN}}{A_{GAP}}\right)^2+\left(\frac{A_{SG}}{A_{GAP}}-\frac{A_{GAP}}{A_{SG}}\right)^2\left(\frac{A_{SEN}}{A_{SG}}\right)^2+\left(\frac{A_{SEN}}{2A_{port}}\right)^2}} \tag{1}$$

where H_1 (m) is the distance between the tundish level and bottom of the tundish, H_2 (m) is the distance from UTN upper edge to the upper edge of SEN port exit, g is the gravitational acceleration (m^2/s), A_{SEN} (m^2) is the SEN inner cross-section area, A_{port} (m^2) is the area of the port exit projected to the liquid steel jet direction, f is the friction factor for turbulent flow in a circular pipe, with an estimated value of 0.075 from the Moody's chart, L_{SEN} (m) is the SEN length, D_{SEN} (m) is the SEN inner diameter, μ is the coefficient of contraction, A_{SG} (m^2) is the area of the slide gate when it is fully opened, and A_{GAP} (m^2) is the area of the gap opening projected in the casting direction, as shown in Figure 1 for the top view.

The gap area is calculated from the opening distance, D, and the two diameters D_1 and D_2, as follows:

$$A_{GAP} = \frac{D_1^2}{4}\arcsin\left(\frac{2h}{D_1}\right)+\frac{D_2^2}{4}\arcsin\left(\frac{2h}{D_2}\right)-Dh, \qquad if \quad D > \frac{\sqrt{D_1^2-D_2^2}}{2} \tag{2}$$

where h is given by:

$$h = \frac{D_1D_2}{4D}\sqrt{1-\left(\frac{D_1^2+D_2^2-4D^2}{2D_1D_2}\right)^2} \tag{3}$$

The two diameters D_1 and D_2 are defined such that $D_1>D_2$, and represent the plate bore diameter and SEN inner diameter, depending on which is larger. As shown in Figure 1, while the two circle centers approach each other during gate opening, D decreases, and the overlapped area becomes larger. If the two diameters, D_1 and D_2, are very different, then for large nozzle opening fractions, D may become small enough that the condition in equation (2) does not hold, and the gap area can no longer be calculated using that equation. However, this scenario is not expected during normal casting operations, so only equation (2) is presented.

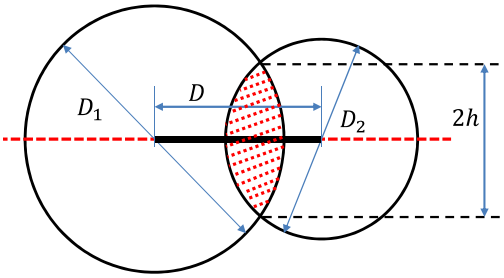

Figure 1. Top View of Gate and SEN Inner Bores

The parameter μ in equation (1) is the ratio between the area of the Vena contracta and A_{GAP}, and is estimated following the equation (3) below [9], note that μ here is not the dynamic viscosity for fluids:

$$\mu = 0.63 + 0.37\left(\frac{A_{GAP}}{A_{SG}}\right)^3 \tag{3}$$

A_{eff} in equation (1) represents the effective area taking into account the gas injection into the system. For single phase flow without gas injection, effective area A_{eff} equals SEN inner cross-section are, A_{SEN}, for the multiphase flow case, A_{eff} takes the form in equation (4):

$$A_{eff} = \frac{V_c WT}{Q_{gas} + V_c WT} A_{SEN} \tag{4}$$

where Vc is the casting speed, W and T are the mold width and thickness respectively.

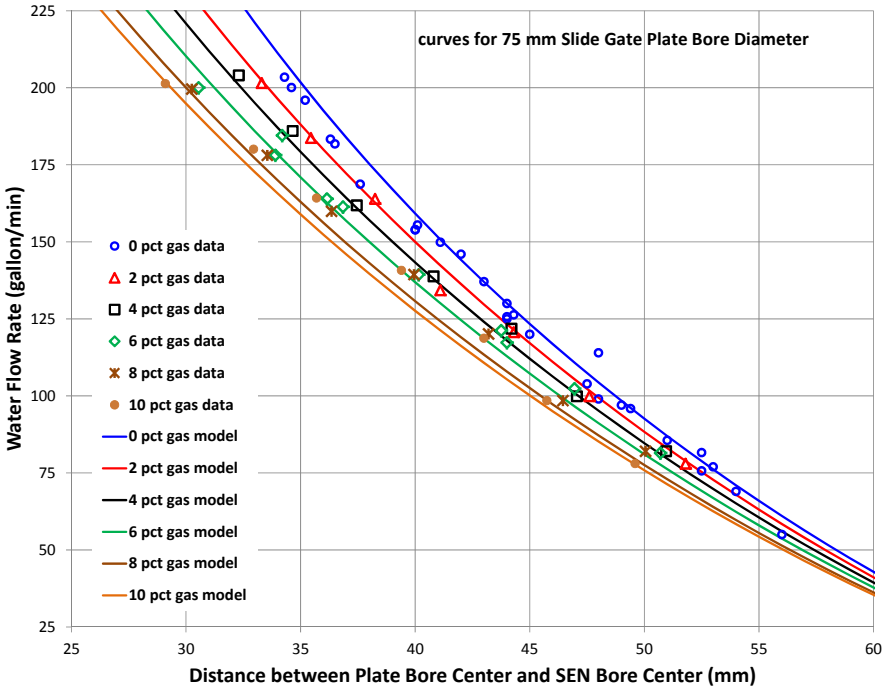

Figure 2. Flow Rate in SEN vs. Slide Gate Opening
(D is used in this figure, as distance between plate and SEN bore centers)

Figure 2 compares the predicted liquid flow rate using the gate-position-based model with the measured slide-gate opening from full-scale water-model experiments performed at ArcelorMittal Global R&D center at East Chicago. The experiments were conducted by recording the slide gate position for a given flow rate, after waiting for the meniscus to stabilize at a certain location. The gas volume fraction was calculated based on the total measured flow rates of gas and liquid. As gas volume fraction increases, for the same liquid flow rate, the slide gate must open wider, in order to accommodate the larger total volume, and overcome the gas buoyancy [1]. This model is validated by noting that the model predictions match very well with the water model measurements for gas volume fractions up to 10%. Because equation (1) is independent of fluid properties, it can be directly applied to calculate liquid steel flow rate in the continuous steel caster.

In addition to its use in the present work to determine the transient flow rate during dithering, this gate-position-based model can be applied directly to predict clogging during the actual casting process. Clogging in the nozzle and SEN will increase the pressure head loss in the system, causing the measured flow rate to decrease relative to the prediction of equation (1). By comparing the predicted and measured flow rates, a clogging parameter can be calculated to indicate the extent of clogging during casting.

Porous-flow Model for Argon Gas Flow Rate Prediction in Hot Condition

Because measuring hot argon flow rate and bubble size distribution is difficult, models have been developed to calculate these important parameters [10], and applied in this work. Assuming laminar flow of argon flow through the UTN refractory so Darcy's law applies, the ideal gas law, and continuity equation for argon are combined to give the following equation for pressure and velocity in the porous refractory walls of the nozzle:

$$\nabla\cdot\left(K_D\nabla p\right)=-\frac{RT}{p}\left[\nabla\left(\frac{p}{RT}\right)\cdot\left(K_D\nabla p\right)\right];\ \mathbf{v}=-K_D\nabla p\ ;\ \text{where}\ K_D=\frac{K_{DS}}{\mu(T)} \tag{5}$$

T is the absolute temperature in (K), R is the gas constant for argon with the value of 208 (J/kg·K), and K_D is the permeability, which is determined by both the specific permeability and the dynamic viscosity. K_{DS} is the refractory specific permeability, given a typical value of 1.01×10^{-12} m^2 in current work, and the temperature-dependent viscosity for argon gas was obtained based on experiments [11], and expressed as:

$$\mu(T)=\mu_0*10^{\left(0.63842\lg T-6.9365/T-3374.72/T^2-1.51196\right)} \tag{6}$$

where μ_0 is the argon dynamic viscosity at 20 °C, and has the value of 2.228×10^{-5} Pa·s.

This porous-flow model has been validated elsewhere [8] both via numerical simulation with test cases, as well as a static water experiment. In this work, this model is utilized to calculate argon flow rate entering liquid steel stream under hot conditions. Gas leakage during injection this makes the hot argon flow rate less than expected, which has a great impact on flow in the mold region, The measured cold gas flow rate (standard conditions), is converted into gas flow rate in hot condition, using the method proposed in [5]. In this method, back pressure is used as the inlet boundary condition to calculate argon gas flow through UTN refractory in hot condition. The measured cold argon flow rate can be used to calculate the gas leakage during the process. The results are input to a two-step model of gas bubble formation to estimate the bubble size distribution, based on previous empirical model of the distribution of active gas-flow sites in the refractory. Details of this porous-flow model are given in [12].

Eulerian-Eulerian Model for Argon-Steel Two-Phase Flow Simulation

Using the results from the above two models, an Eulerian-Eulerian model has been developed to solve the Navier-Stokes equations for both argon and liquid steel phases respectively in this work. The governing equation for mass conservation is shown in equations (8) and (9) below [13]:

$$\frac{\partial\left(\alpha_a\rho_a\right)}{\partial t}+\nabla\cdot\left(\alpha_a\rho_a\mathbf{v}_a\right)=0 \tag{8}$$

$$\frac{\partial\left(\alpha_s\rho_s\right)}{\partial t}+\nabla\cdot\left(\alpha_s\rho_s\mathbf{v}_s\right)=0 \tag{9}$$

Governing equations for momentum conservation of the system writes in equation (10) and (11) below [FLT]:

$$\frac{\partial\left(\alpha_a\rho_a\mathbf{v}_a\right)}{\partial t}+\nabla\cdot\left(\alpha_a\rho_a\mathbf{v}_a\mathbf{v}_a\right)=-\alpha_a\nabla p+\nabla\cdot\left(\alpha_a\mu_a\nabla\mathbf{v}_a\right)+K_{as}\left(\mathbf{v}_s-\mathbf{v}_a\right)+\alpha_a\rho_a\mathbf{g} \tag{10}$$

$$\frac{\partial\left(\alpha_s\rho_s\mathbf{v}_s\right)}{\partial t}+\nabla\cdot\left(\alpha_s\rho_s\mathbf{v}_s\mathbf{v}_s\right)=-\alpha_s\nabla p+\nabla\cdot\left(\alpha_s\left(\mu_s+\mu_t\right)\nabla\mathbf{v}_s\right)+K_{as}\left(\mathbf{v}_a-\mathbf{v}_s\right)+\alpha_s\rho_s\mathbf{g} \tag{11}$$

The coefficient K_{as} in the equations above reflects the interfacial drag forces between argon and liquid steel, which is calculated following equation (12) [12].

$$K_{as} = \frac{3}{4}\frac{C_D}{D_b}\alpha_s \rho_s \left|\mathbf{v}_s - \mathbf{v}_a\right|, \text{ where } \quad C_D = \frac{24}{\mathrm{Re}_b}\left(1+0.15\,\mathrm{Re}_b^{0.687}\right), \quad \mathrm{Re}_b = \frac{\rho_s \left|\mathbf{v}_s - \mathbf{v}_a\right| D_b}{\mu_s} \tag{12}$$

D_b in equation (12) is the bubble diameter, and expression for the drag coefficient C_D is from [14].

The standard k-ε model was applied on the liquid steel phase via solving for the turbulence kinetic energy, k, and dissipation rate, ε, from another two separate sets of equations. The turbulent eddy viscosity is then calculated based on equation (13) below:

$$\mu_t = C_\mu \rho_s \frac{k^2}{\varepsilon} \tag{13}$$

where C_μ is a constant taking the value of 0.09.

The argon gas phase and liquid steel phase share the same pressure field. Finally, the volume fractions of the liquid steel and argon must satisfy equation (14):

$$\alpha_s + \alpha_a = 1 \tag{14}$$

Boundary conditions include prescribed liquid steel velocity into the upper tundish nozzle above the slide gate to satisfy the flow rate, hot gas velocity distribution and average bubble size at UTN inner surface, pressure outlet conditions at the bottom of the mold region, and standard wall laws at other surfaces. The meniscus is treated as a no-slip wall, owing to the highly-viscous slag layer. The mold level is calculated based on local pressure at the top surface. Mass and momentum sinks are added at cells adjacent the shell interface to account for the solidification of liquid steel that moves downward at the casting speed and at cells adjacent to the meniscus to account for the escape of argon gas, based on a zero velocity gradient assumption.

MODEL VALIDATION

In order to validate the mesh strategy, turbulence model, and discretization scheme used in the dithering simulation and other model applications, water model experiments were performed for single phase flow and measurements of sub-meniscus horizontal velocities were compared with simulation results, using the domain shown in Figure 3.

Full-Size Water-Model Experiments

The experiments were conducted at ArcelorMittal Global R&D Center at East Chicago, using impeller sensors to measure velocity at 9 different locations across the mold width direction. The sensors were positioned at the center plane between mold broad faces, at 50 mm below the free surface. The curved water model mold/strand width is 56 inches, and thickness is 235mm. Submergence depth of the SEN is fixed at 8 inches from free surface to the upper edge of the round SEN ports, which were angled 15^o downwards. No argon was injected. Velocities were measured for four casting speeds in the experiments, with 25, 35, 45 and 55 ipm (inches per minute). Each measured data point in Figure 4 is the mean velocity averaged over 3 min. Increasing the casting speed is found to increase the surface water velocity accordingly. As expected, classic double-roll flow patterns were found in all four cases.

Computational Model Details

These water model experiments were simulated using a single-phase simplification of the computational model. The domain includes half of the curved mold and strand, as shown in Figure 3(a), assuming symmetric flow between sides. To ensure efficient convergence and accuracy, both the SEN and mold region are divided into blocks with mapped hexahedral cells. The mesh blocks for the SEN are shown in Figure 3(b), and final mesh composed of 0.6 million mapped hexahedral cells for the computational model is in Figure 3(c).

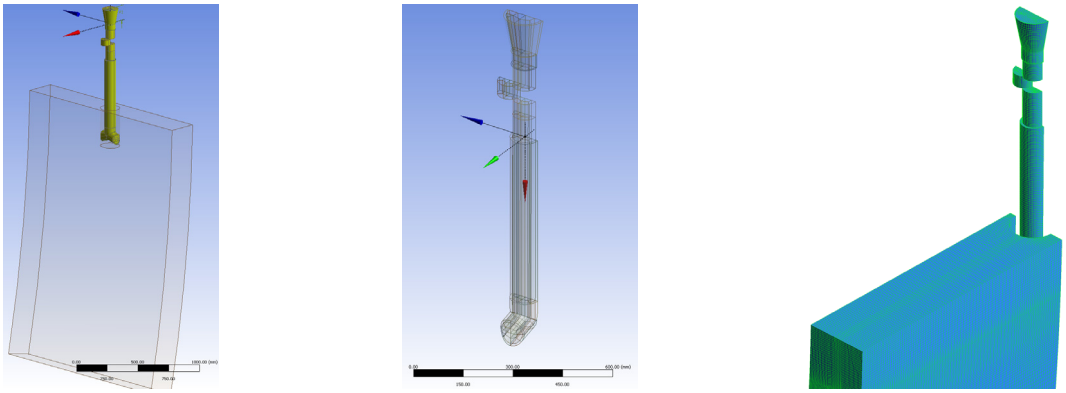

(a) Domain Geometry (b) Mesh Blocks (c) Hexahedral Meshes

Figure 3. Model Geometry and Mesh for Water Model Simulation

Two turbulence models, a standard k-ε model (with solid lines) and a Reynolds Stress Model (RSM, with dashed lines, for cases with 25 and 55 ipm casting speeds), were adopted to simulate cases with casting speeds of 25 ipm to 55 ipm for comparison. The 1st order upwind scheme was utilized for discretization. Despite the fact that the 1st order upwind scheme is notorious for its numerical diffusion, recent work shows that this scheme calculates jet velocities that match well with measured jet velocity profiles, because the extra jet spread produced by the false diffusion associated with 1st order upwinding compensates the generally narrower jet produced with the k-ε model [7].

Model Evaluation

The measured and simulated surface velocities in the water model in Figure 4 match very well for all cases, as shown in Figure 4. Simulation results with the standard k-epsilon turbulence model consistently show a slight under-prediction of the surface horizontal velocity at mold quarter point. Using the RSM model produces slightly better agreement. However, the RSM model must solve transport equations for all six independent Reynolds stress components, so its computational cost is much higher than the standard k-ε model, which only solves two equations for turbulence kinetic energy k and its dissipation rate ε. The results in Figure 5 suggest that as casting speed increases, the under-prediction of surface velocities with the standard k-ε model becomes less obvious. In the dithering simulation, with a the average casting speed is 40 ipm, corresponding to 55 ipm in the water model. At this casting speed, the predictions of the standard k-ε model with 1st order upwinding scheme agree very well with the measurements. Thus, this model is chosen for subsequent simulation of argon-steel flow during slide-gate dithering.

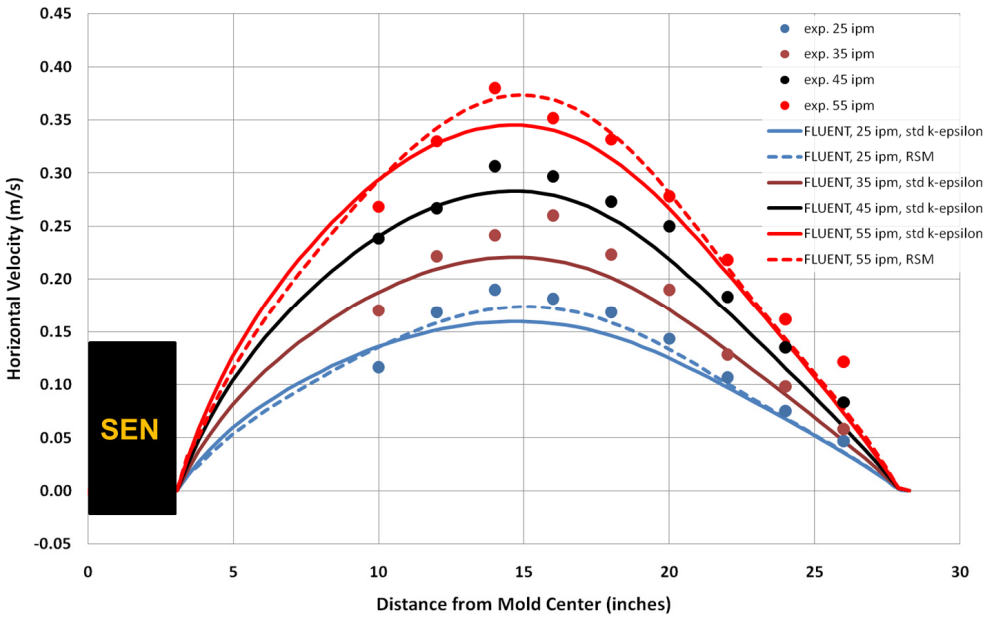

Figure 4. CFD Model Validation with Water Model Experiment

RESULTS: SLIDE-GATE DITHERING APPLICATION

The validated computational models were applied to simulate the effects of slide-gate dithering on fluid flow in the caster. First, the slide-gate position history measured at the plant is converted into the flow-rate history entering the nozzle, for a 40sec time interval that included a transition between two dithering conditions during multiphase flow. Next, the porous-flow model was used to calculate the argon flow rate into the molten steel stream under hot conditions, taking into account predicted gas leakage, and the bubble distribution was calculated. These results define the time-dependent inlet conditions to the UTN. Then, the Eulerian-Eulerian multiphase flow model with standard k-ε model was applied to simulate turbulent flow in the nozzle and mold during the dithering event, to reveal the evolving transient flow patterns in SEN and mold region. Finally, the mold level history is predicted with a simple pressure method, and compared with the unfiltered mold level signal measured during the time interval.

Gate-Position Model Flow-Rate Results

The measured slide-gate position and mold-level signals are plotted in Figure 7, with a sampling rate of 0.05sec. From time 120 sec to 180 sec, the slide gate was oscillated at a frequency of 0.4 Hz, with a stroke of 14 mm; from time 180 sec, the dithering stroke was decreased to 7 mm, (same frequency); and from time 212 sec, the dithering frequency was increased to 0.8 Hz (same stroke).

The simulation started at time 160 sec and ends at time 200 sec, as indicated by the vertical red dashed lines in Figure 7, with a time span of 40 sec. The curve shown in Figure 8 (a) is calculated from the gate-position-based model, with a 6% argon gas volume fraction, (see porous-flow model results). The liquid steel flow-rate history calculated during dithering is shown in Figure 8(b), where a flow rate change takes place at 180sec from 83 gpm (with 14 mm dithering stroke), to 38 gpm flow rate (with 7 mm dithering stroke). The converted inlet liquid steel velocity history is also plotted in Figure 8(b).

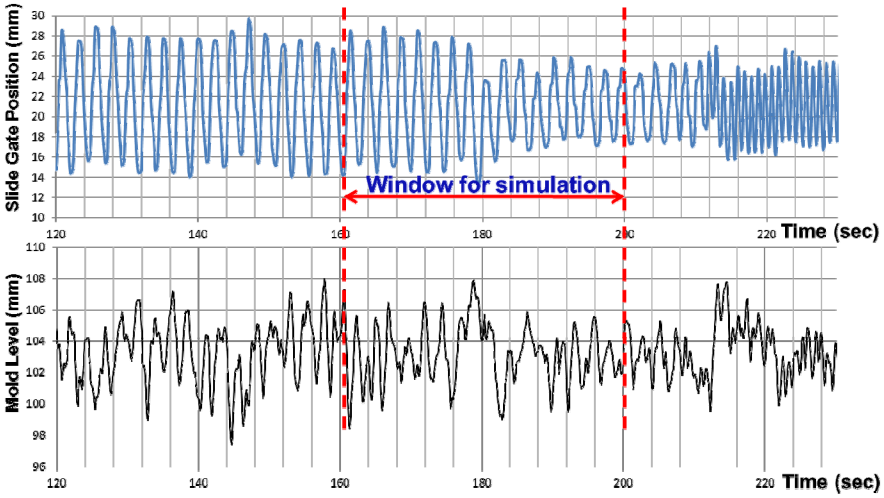

Figure 7. Measured Slide-gate Position and Mold Level History

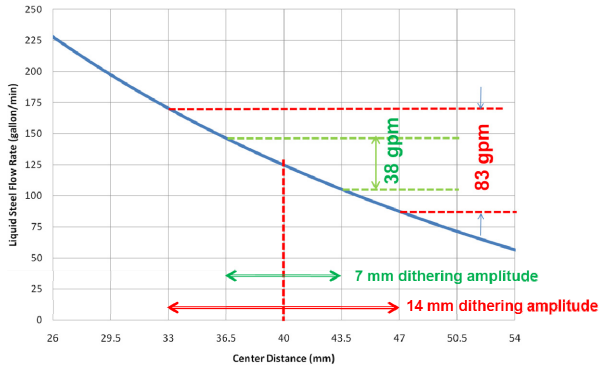

(a) Flow Rate vs. Gate Opening Curve for 6% Gas

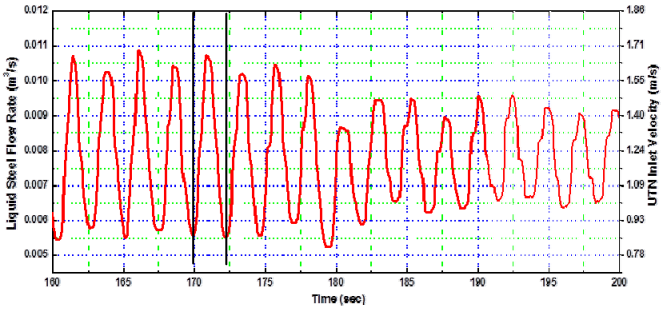

(b) Inlet Liquid Steel Flow Rate History

Figure 8. Inlet Liquid Steel Flow Rate Calculation based on Gate-position-based Model

Porous-Flow Model Results

The porous-flow model predicts that 30 LPM of argon gas enters the UTN, (at ~1550 ^{o}C and ~85kPa), which represents a 6% volume fraction, based on a casting speed of 40 ipm for this mold. The average bubble size was 2.4mm. The simulation was based on the measured back pressure of 19psi, and compares with 20 LSPM cold argon flow rate, recorded in the process data. These results correspond to 75% argon gas leakage. Although not directly validated, mold flow computations that neglected leakage predicted a single-roll flow pattern which is known not to be observed in the plant.

Eulerian Flow Model – Initial Flow Pattern

The Eulerian-Eulerian two phase flow model is first used to calculate the steady state velocity distribution as the initial field for the dithering simulation, based on the hot argon flow rate calculated from the porous-flow model, and a liquid steel flow rate of ~0.0061 m^3/s, representing conditions at 160sec during the dithering trial. The computational domain is half of the nozzle and mold region, extending to 3m below the meniscus. The domain contains only the liquid pool, as its boundary is defined by the interface with the solidifying shell, as shown in Figure 6(a). The mesh consists of 1 million mapped hexahedral cells (Figure 6(b)).

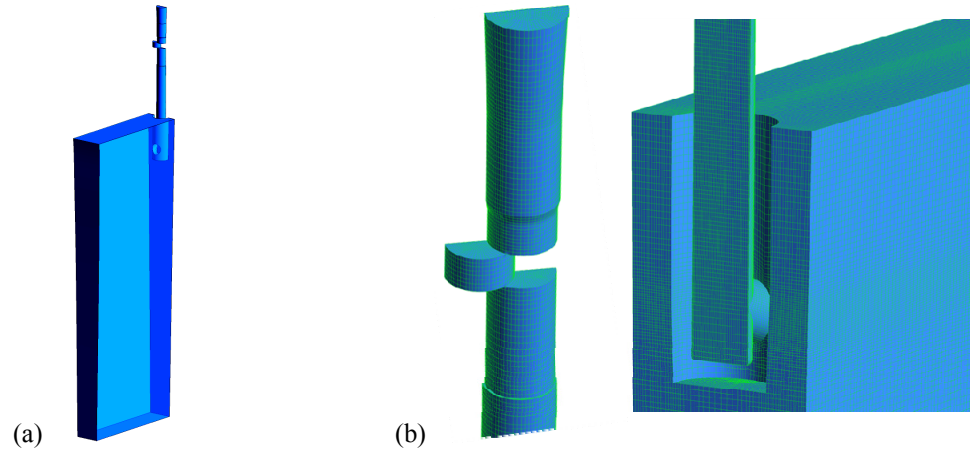

(a) (b)

Figure 5. Geometry and Mesh of Caster Domain

Operation parameters for the dithering process and simulation are listed in Table I below.

Table I. Operation Parameters for Dithering Process

Inlet Steel Velocity (m/s)	Mold Width (inch)	Mold Thickness (inch)	Dithering Stroke (mm)	Dithering Frequency (Hz)
0.96	72	10	14 changed to 7	0.4
Plate Bore Diameter (mm)	SEN Inner Bore Diameter (mm)	Mold Level Sampling Rate (per sec)	SEN Submergence Depth (inch)	
75	80	1/0.05	8	

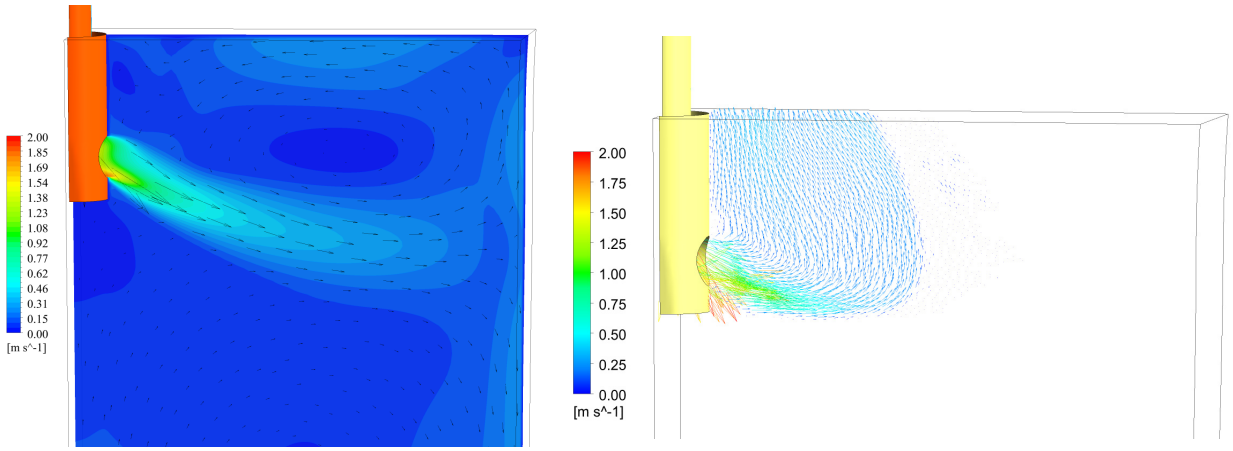

(a) Liquid Steel Velocity Distribution (b) Argon Gas Velocity Distribution

Figure 6. Initial Flow Field for Liquid Steel and Argon Gas

The calculated liquid steel and argon gas flow patterns are shown in Figure 6. A double-roll flow pattern is found, which is consistent with surface velocity observations. The argon gas velocity distribution at center plane between broad faces is plotted in Figure 6(b). Most of the gas separates from the steel jet soon after leaving the nozzle port, rising upwards to exit the top surface near to the SEN.

Nozzle and Mold Flow Model – Transient Results

Evolution of transient liquid steel flow and argon gas distribution in the nozzle and mold was simulated with the transient Eulerian-Eulerian multiphase flow model, starting from the steady-state solution as the initial condition, using a 0.05sec time step size. The flow rate history was taken from the gate-position-based model, for the time interval from 160 – 200sec, which contains the change in dithering conditions at 180sec from 14mm to 7mm stroke. This flow rate is applied as the inlet velocity boundary condition to the top or the UTN, and the argon gas velocity and bubble size from the porous-flow model is applied to the UTN side walls.

Results are presented in Figure 9 to 12 for a typical dithering cycle from 170 to 172 sec (indicated by the vertical dotted lines in Figure 8b). Figure 9 displays the liquid steel velocity distribution at SEN port exit, projected to the horizontal direction. Most of the liquid exits the port bottom, owing to the downward momentum of the nozzle flow, and the typical oversized port area, which is 2.0 times

the nozzle bore area. In addition, a strong swirling is observed. This swirling phenomenon is caused by the blocking effect of the slide gate. Asymmetric liquid steel flow is produced below the partially-open slide gate in the SEN. This downward velocity along the north side of the SEN generates a strong counterclockwise swirl at the SEN bottom, (viewed looking into the west port) and this swirl is sustained through port exits into the liquid pool in the mold.

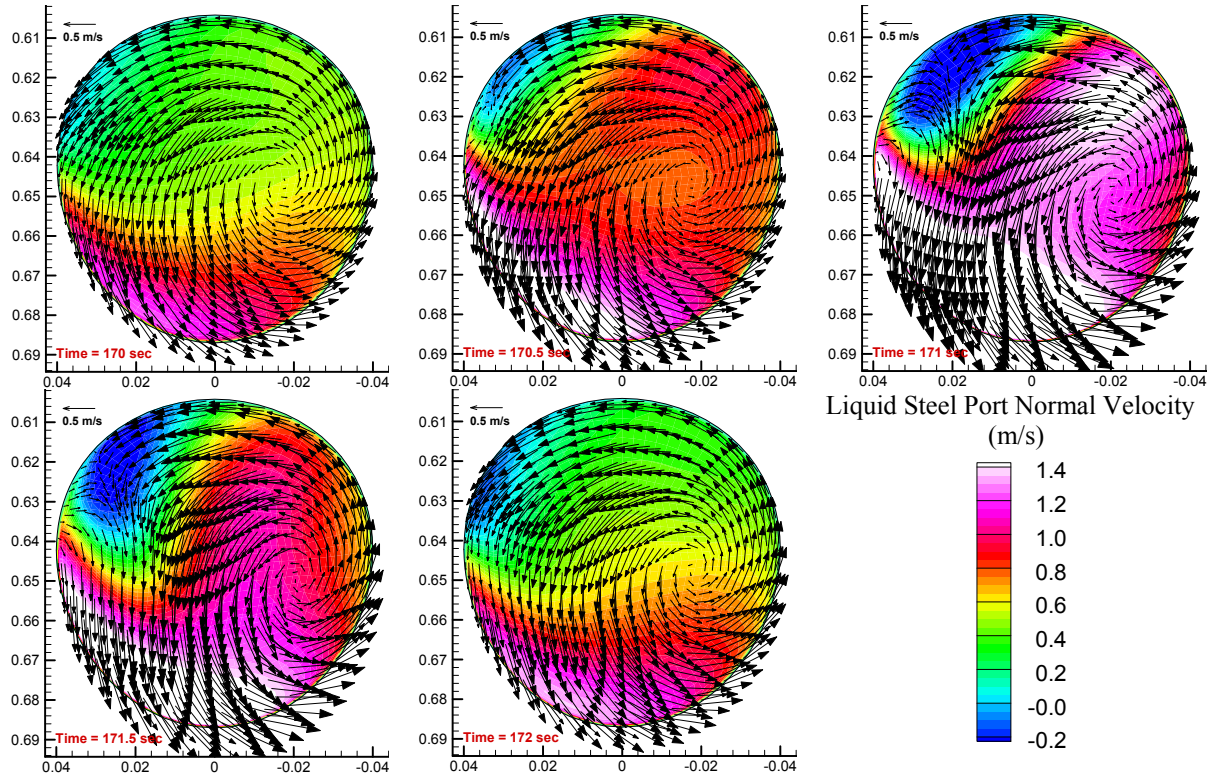

Figure 9. Liquid Steel Velocity Distribution at SEN Port Exit, axis in (m)

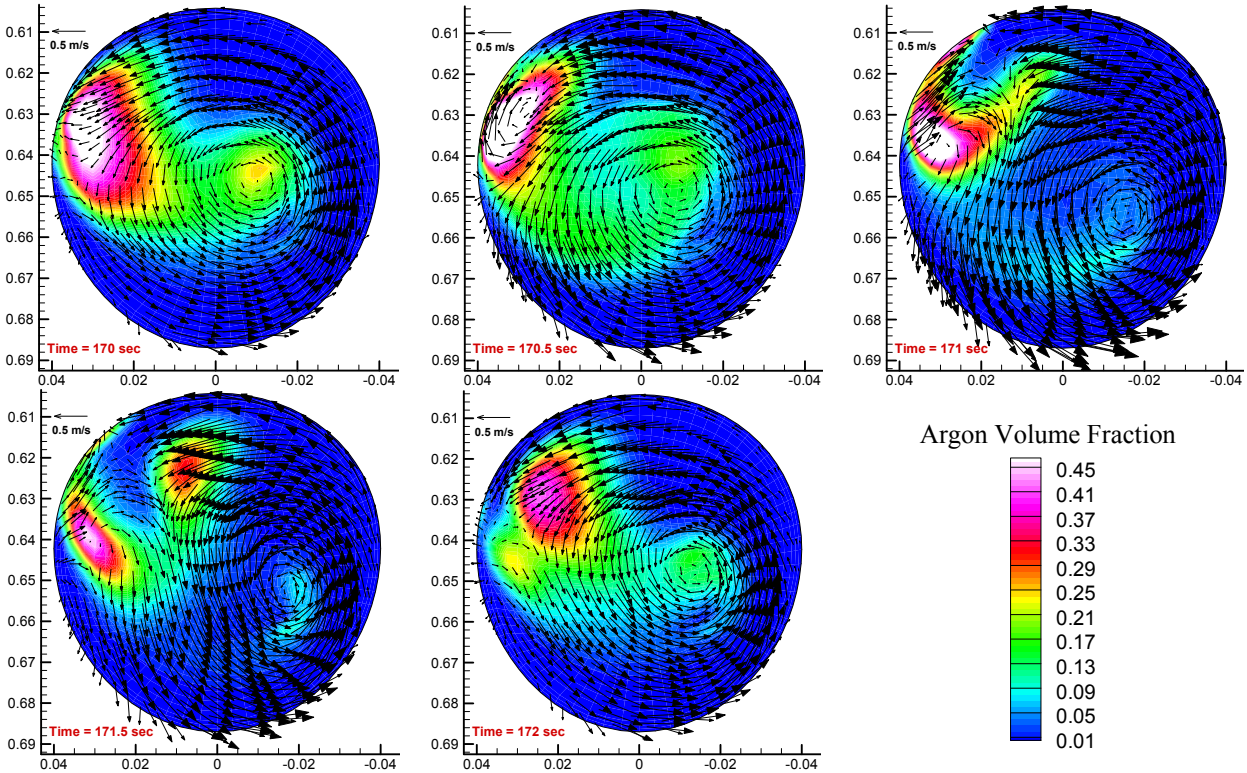

Figure 10. Evolving of Argon Velocity and Concentration Distribution at SEN Port Exit, axis in (m)

Argon gas velocity and volume fraction distributions through the dithering cycle (170 to 172 sec) are exhibited in Figure 10. The argon enters the mold cavity mainly from the upper left region of the port exit, where its volume fraction exceeds 45%, and generally from around the center of the port, where it is 10% - 20%. This is because the steel flow exits more from the bottom and outside right regions of the port, and the low-density, low-momentum argon flow concentrates in the opposite regions.

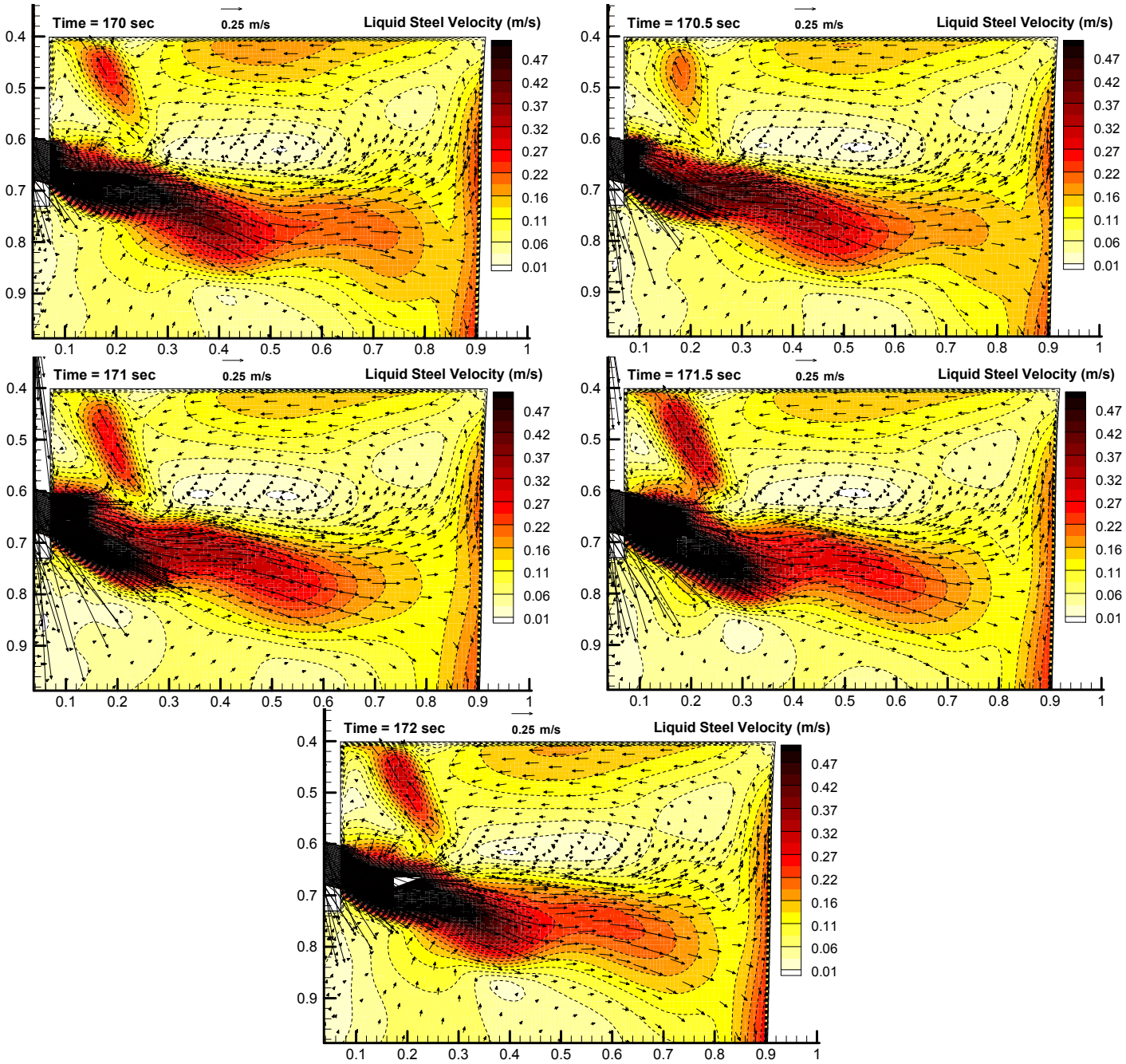

Figure 11. Evolving of Liquid Steel Velocity Distribution at Center Plane during Dithering, axis in (m)

The transient fluctuations of the jet during the example dithering cycle are illustrated in Figure 11. The jet generally enters the mold cavity at ~20^0 downward, which is slightly steeper downward than the port angle. In addition, the strong swirling flow sends flow upwards from the upper port, creating a "nose" in the jet profile entering the mold cavity. This swirl and nose is most prominent during the time of maximum flow rate, which is experienced midway through the dithering cycle, at ~171 sec. The increase in flow rate, which occurs during the first 3 frames of this figure, causes the jet in the mold cavity to "wobble". This generates fluctuations in the flow pattern, in addition to an overall increase in velocity in the mold cavity. Later in the cycle, (eg. 172sec), as the flow rate decreases, the jet tends to straighten out.

The behavior of the argon gas in the mold is shown in Figure 12. Periodic variation of the liquid steel flow from the dithering causes accompanying variations in the argon gas fraction of the flow, which injects high-concentration gas "pockets" into the mold at the same frequency of ~2.5sec. These gas pockets contain ~25-50%gas. The high buoyancy of these gas pockets causes them to leave the jet at float directly to the top surface, which takes ~5sec. Because this period is roughly double the injection frequency, there are usually two gas pockets observed in the mold cavity at any instant in time. One gas pocket is just emerging from the port, and another is still rising to the surface from the previous cycle. The gas pocket elongates as it rises, producing the higher-velocity plume next to the SEN in the frames of Figure 11.

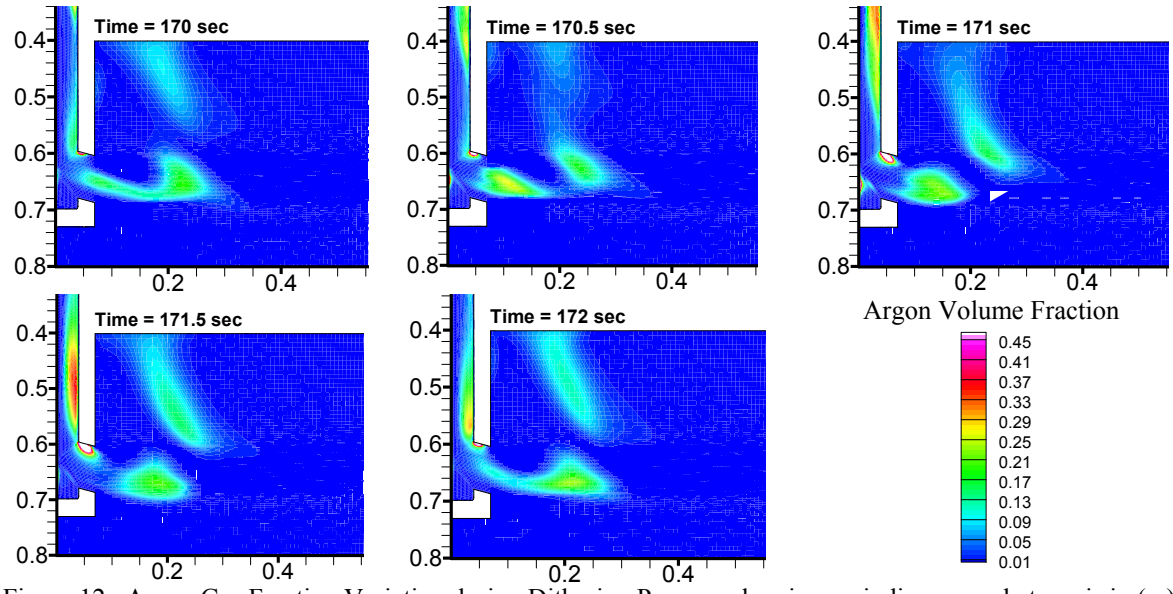

Figure 12. Argon Gas Fraction Variation during Dithering Process, showing periodic gas pockets, axis in (m)

Mold-Level Results

Periodic change of liquid steel flow rate during dithering process also affects the mold level profile and fluctuations at the top surface. In this simulation, a flat wall is imposed at the top surface, so to predict mold level, a simple pressure calculation is used:

$$\Delta h = \frac{p - p_0}{\rho_L g} \tag{15}$$

where Δh is the mold level deviation, p is the pressure at top surface, and p_0 is the pressure corresponding to the reference mold level used in determining Δh. ρ_L is the liquid density, and g is the gravitational acceleration. Displacement of the liquid slag layer is neglected in this equation, because the entire layer was judged to be thin enough to simply rise and fall with the steel surface profile variations. A comparison between the predicted mold level during the simulated 40 sec of dithering and the measured unfiltered mold level data is shown in Figure 13.

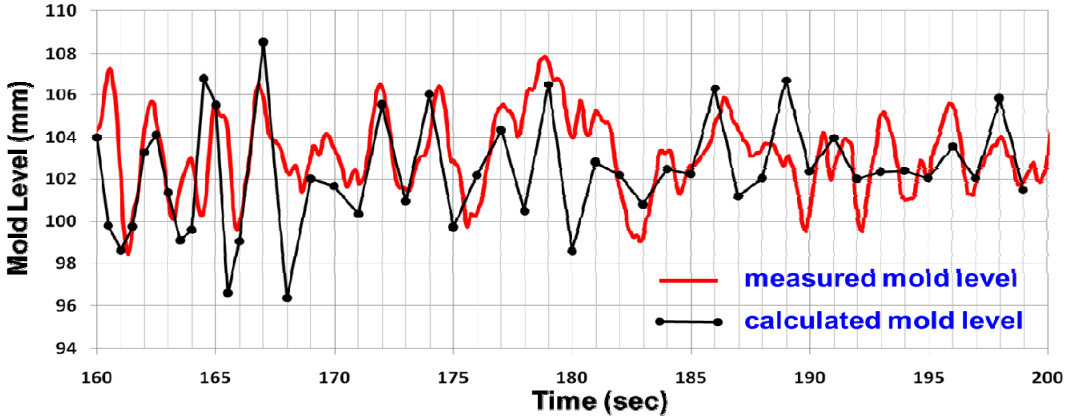

Figure 13. Comparison between Calculated and Measured Mold Levels at Quarter Mold Point

Excellent agreement between the predicted and measured mold level is found in Figure 13, with both the level fluctuation magnitude and phase matching very well with each other. Both the prediction and measurement show smaller mold level fluctuations when the dithering stroke is decreased. Specifically, the measured level fluctuations decrease from 4.7mm to 2.7mm. The mold level fluctuation frequency roughly matches the dithering frequency of 0.4 Hz. As the casting speed stays constant, and the amplitude and frequency of the level fluctuations relates directly to the dithering stroke and frequency, simple mass conservation over the whole system is the main phenomenon controlling surface level variations during this dithering process, especially when dithering stroke is large. Secondary phenomena involve the feedback caused by reinforcement of the flow in the upper recirculation zones, gravity waves, and mold level oscillations, which will be investigated in future work with this model to optimize the dithering process.

CONCLUSIONS

A system of models was developed and validated in this work to model the slide-gate dithering process, including a gate-position-based model for SEN liquid steel flow rate prediction, a porous-flow model to estimate hot argon flow rate injected into UTN, and an Eulerian-Eulerian model to simulate argon-steel two phase flow in both SEN and mold region during dithering with inlet boundary conditions provided by previous models. The models were validated by matching velocity measurements in a water model, and applied to reach the following conclusions:

1. The calculated mold level using the system of models presented here matches with plant measurements during transient dithering experiments, which tends to validate the new submodels, and the pressure method for estimating surface profile.
2. Mold level oscillates periodically during dithering, with about the same frequency as the dithering frequency, and the level fluctuations decrease from ~5mm to ~3mm for dithering stroke decreasing from 14mm to 7mm;
3. Liquid steel jet wobbling and periodic argon gas-rich "pockets" entering mold region through SEN port exits are observed in the simulation of the dithering process;
4. Although the current model ignores the effects of sloshing, mold oscillation, and small-scale turbulent eddies, it is already a useful tool for optimization of dithering and other transient phenomena in future work.

ACKNOWLEDGMENT

The authors thank the members of the Continuous Casting Consortium at the University of Illinois at Urbana-Champaign for support of this research, and we want to thank Kai Zheng and Bill Umlauf at ArcelorMittal Global R&D in East Chicago for providing the mold level measurement data.

REFERENCES

1. H. Bai and B.G. Thomas, "Effects of Clogging, Argon Injection and Continuous Casting Conditions on Flow and Air Aspiration in Submerged Entry Nozzle", *Metallurgical and Materials Transactions B*, Vol. 32B, No. 4, 2001, pp. 707-722

2. L.C. Hibbeler and B.G. Thomas, "Mold Flux Entrainment Mechanisms", BAC 2010, Fourth Baosteel Biennial Conference Proceedings, Shanghai, PRC, 2010, pp. B83-90.

3. Y. Wang and L. Zhang, "Study on Transient Fluid Flow Phenomena during Continuous Casting: Part II: --Cast Speed Change, Temperature Fluctuation, and Steel Grade Mixing", *ISIJ International,* Vol. 50, No. 12, 2010, pp. 1783-1791.

4. R. Liu, J. Sengupta and B.G. Thomas, et.al., "Effects of Stopper Rod Movement on Mold Fluid Flow at ArcelorMittal Dofasco's No. 1 Continuous Caster*", AISTech 2011*, Indianapolis, IN, May 2-5, 2011

5. X. Huang and B.G. Thomas, "Modeling of Transient Flow Phenomena in Continuous Casting of Steel", *Canadian Metallurgical Quarterly*, Vol. 37, No. 304, 1998, pp. 197-212.

6. Yuan, Q., B. G. Thomas, and S. P. Vanka, "Study of Transient Flow and Particle Transport during Continuous Casting of Steel Slabs, Part 1. Fluid Flow," *Metallurgical and Materials Transactions B*, Vol. 35B:4, 2004, pp. 685-702.

7. Chaudhary, Rajneesh, Surya P. Vanka, and Brian G. Thomas "Transient Turbulent Flow in a Liquid-Metal Model of Continuous Casting, Including Comparison of Six Different Methods", *Metallurgical and Materials Trans. B*, Vol. 42B: 5, 2011, pp. 987-1007.

8. T. Shiand B.G. Thomas, "Effect of Gas Bubble Size on Fluid Flow in Continuous Casting Mold", Continuous Casting Consortium at University of Illinois at Urbana-Champaign, Report, 2001.

9. H. Oertel, L. Prandtl, et.al, "Prandtl's Essentials of Fluid Mechanics", *Springer*, ISBN 0387404376. pp. 163–165.

10. R. Liu, B.G. Thomas and J. Sengupta. "Model of Argon Flow through UTN Refractory and Bubble Size Estimation", Continuous Casting Consortium at University of Illinois at Urbana-Champaign, Report, 2011.

11. R. Dawe and E. Smith, "Viscosity of Argon at High Temperatures", *Science*, Vol. 163, 1969, pp. 675-676.

12. H. Bai and B.G. Thomas, "Bubble Formation during Horizontal Gas Injection into Downward Flowing Liquid", *Metallurgical and Materials Transactions B*, Vol. 32B, No. 6, 2001, pp. 1143-1159.

13. FLUENT ANSYS Inc. 2007 FLUENT 6.3-Manual (Lebanon, NH).

14. L. Schiller and Z. Naumann. *Verhandlungen der Deutschen Ingenieur,* Vol. 77, 1935, pp318.